Tracking oxidation-induced alterations in fibrin clot formation by NMR-based methods

Wai Hoe Lau
Lee Kong Chian School of Medicine, Nanyang Technological University, Singapore
Nathan J. White
Department of Emergency Medicine, University of Washington School of Medicine, Seattle, Washington
Tsin Wen Yeo
Communicable Diseases Centre, Institute of Infectious Disease and Epidemiology, Tan Tock Seng Hospital, Singapore
Russell L. Gruen
ANU College of Health and Medicine, The Australian National University, Canberra ACT, Australia
Konstantin Pervushin (kpervushin@ntu.edu.sg)
School of Biological Sciences, Nanyang Technological University, Singapore

Research Article

Keywords: oxidation, fibrin clot formation, coagulation factors

Posted Date: March 19th, 2021

DOI: https://doi.org/10.21203/rs.3.rs-308964/v1

Version of Record: A version of this preprint was published at Scientific Reports on August 3rd, 2021. See the published version at https://doi.org/10.1038/s41598-021-94401-3.

Abstract

Plasma fibrinogen is an important coagulation factor that is susceptible to post-translational modification by oxidants. We have reported altered fibrin polymerization and increased methionine oxidation in fibrinogen after exposure to hypochlorous acid (HOCl), and similarly in the fibrinogen of severely injured trauma patients. Molecular dynamics suggests that methionine oxidation offers a mechanistic link between oxidative stress and coagulation through fibrin protofibril lateral aggregation by disruption of AαC domain structures. However, experimental evidence explaining how HOCl oxidation impairs fibrinogen structure and function has not been demonstrated. We used polymerization studies and two dimensional-nuclear magnetic resonance spectrometry (2D-NMR) to test the hypothesis that HOCl oxidation alters fibrinogen conformation in the prefibrillar state and T_2 water surface relaxation of fibrin fiber assemblies. We found that both HOCl oxidation of purified fibrinogen and addition of HOCl-oxidized fibrinogen to plasma disrupted fibrin polymerization similarly to competitive inhibition of polymerization using a recombinant AαC fragment (AαC 419–502). DOSY NMR measurement of ^{1}H fibrinogen at 25^{o}C demonstrated that fibrinogen oxidation increased translational diffusion coefficient by 17.4%, suggesting a more compact and rapidly translational motion of the protein with oxidation. 2D-NMR analysis of control plasma fibrin gels indicated that water existed in two states, namely intermediate (T_{2i}) in the hydration shell of fibrin fibers, and bulk (T_2) within the gel. T_2 relaxation of bulk water protons was decreased 2-fold in oxidized fibrin gels and was inversely proportional to gel fiber density (T_2). The fast exchange of water protons between hydration shell (T_{2i}) and bulk water, indicating oxidation increased fiber hydration and formed densely packed fibrin gels. We have confirmed experimentally that HOCl oxidation affected native fibrinogen and fibrin gel structures and have demonstrated that NMR can serve as a valuable tool to probe the oxidative rearrangement of fibrin clot structure.

Introduction

Fibrinogen is a 340 kDa glycoprotein, physiologically present in blood plasma at concentrations from 2 to 4 g/L, that self-associates to form the fibrin clot at wounds after its activation by thrombin[1]. It is composed of two pairs of three non-identical chains Aα, Bβ, and γ connected with 29 disulfide bonds. Together, the chains comprise a symmetrical molecule consisting of one globular E region flanked on each side by globular D regions that are connected by three-stranded alpha-helical coiled coils[2,3]. Fibrin is formed by thrombin-mediated proteolytic cleavage and removal of N-terminal fibrinopeptides from the respective Aα and Bβ chains. The exposed binding sites of α- and β- “knobs” are complementary to a- and b- “holes” in the γ and β nodules in the D regions of adjoining monomers. Knob-hole associations each result in the formation of half-staggered, double-stranded protofibrils, which then associate laterally to form fibrin fibers, and ultimately the branching hydrogel network structure of the hemostatic clot[4]. Lateral association is contributed to by interactions between αC regions of the fibrin monomers (αC-αC interactions) during polymerization, which is important for mechanical stiffness, stability, and durability of fibrin clots[5–7]. Polymerization of fibrinogen lacking its αC regions is delayed but not completely inhibited[7].

Fibrinogen is also highly susceptible to many post-translational modifications (PTMs), especially from oxidants and free radicals[3]. One potentially important source of oxidative fibrinogen PTMs has been identified in trauma patients having impaired clot formation[13]. Neutrophils are recruited to the blood after trauma and are activated to release histones and DNA as neutrophil extracellular traps (NETs) and myeloperoxidase (MPO), which synthesizes HOCl by the MPO/ hydrogen peroxide (H_2O_2) oxidant system[8]. HOCl is predominantly generated in the plasma, where it can oxidize methionine residues to methionine sulfoxide as a host-mediated bacterium killing mechanism[9]. Recent evidence supports an important role for fibrinogen in the regulation of these responses by sequestering histones as histone-fibrinogen complexes[10]. We have previously reported that exposure of fibrinogen to HOCl *in vitro* has profound effects upon fibrin polymerization, producing weak, soft, and thin fibered fibrin clots that are resistant to enzymatic degradation by the protease plasmin[11]. We found that methionine at positions AαM476, BβM367, and γM78 were oxidized to methionine sulfoxide by HOCl, though the AαC

domain was preferentially oxidized[11]. Molecular dynamics (MD) simulation revealed that oxidation within the AαC domain may promote opening of key beta-hairpin structures making αC domain dimerization energetically unfavorable in comparison with native structures[12,13]. These data suggest a relationship and potential mechanism by which PTMs by oxidants generated in the blood after trauma can contribute directly to impaired clot formation. This is potentially significant because the risk of death for trauma patients presenting with impaired clot formation is increased up to 6-fold[14].

NMR is an important and useful tool for assessing the structure of gels by examining the movement of water molecules which can be affected by fibrillar structures, cells, vessels, extracellular matrix, and other macromolecules contained therein[15]. Parameters including spin-lattice (T_1) relaxation and spin-spin (T_2) relaxation time and diffusion coefficients can be used to identify important structural characteristics[15,16]. Molecular fingerprints of complex biological fluids such as blood have been encoded using two-dimensional (2D) T_1/T_2 correlations. NMR relaxometry has been used to investigate oxygenated (oxy-Hb), deoxygenated (deoxy-Hb) and oxidized (oxidized Hb) hemoglobin (Hb) derivatives with respect to their altered T_1/T_2 relaxation states[17]. Spin-spin (T_2) relaxation times have also been used to probe fibrin clot structure via paramagnetic properties of hemoglobin in erythrocytes entrapped within whole blood clots[18–20].

In this investigation, we explored HOCl-induced alterations of fibrinogen and fibrin clots using NMR-based methods including a high polarizing magnetic field strength above 600 MHz as well as portable NMR device operating at 80 MHz. One of our goals was to establish the detection limit of the NMR applications to track blood clot structure alterations which can be associated with pathology in blood clot formation or coagulopathy. We hypothesized that HOCl-induced fibrinogen oxidation alters fibrinogen in the prefibrillar state and alters fibrin gel properties that are detectable using NMR methods. To test this hypothesis, we used polymerization studies and NMR to determine ^1H relaxation and translational diffusion properties of fibrinogen solutions and fibrin gels upon oxidation. We report evidence that T_2 relaxation using NMR devices operating at both 80 MHz and 600 MHz describe the changes of fibrinogen conformation and rearrangement of fibril networks after oxidation. Since NMR spectrometer operating at 80 MHz are portable, we foresee that NMR-based methods can be further developed as a potential mobile diagnostic tool to assess the prospect of coagulopathy via detecting alterations of fibrin clot structure due to oxidation *in situ*.

Results

Oxidation alters fibrin polymerization similarly to inhibition of Aα C domain interactions.

During fibrin polymerization, fibrinogen monomers are assembled into double-stranded protofibrils by non-covalent interaction, and these bundle into fibers that branch to form fibrin clot networks[1]. Fibrin clot turbidimetry is useful to examine these polymerization events including the rate of fibrinopeptide cleavage, protofibril formation, and lateral assembly of protofibrils to form fibers[21]. Robust fibrin polymerization representing rapid fibrinopeptide cleavage, protofibril formation, and thick fibrin fibers are represented by turbidity curves having short lag times, steep slopes, and high maximal turbidity. Therefore, we chose turbidity assays to explore the effects of oxidation on fibrin polymerization kinetics. Fibrin formation was initiated by thrombin in the presence of 2 mM calcium in physiological buffer. As shown in Fig. 1a, increasing HOCl concentration increased lag time, decreased slope, and decreased maximal turbidity (Fig. 1a). The maximum rate of lateral aggregation of protofibrils was decreased in a dose-dependent manner (Fig. 1b). Fibrin gel formation became significantly altered by 75 μM HOCl oxidation, with 41% decrease of the rate of polymerization as compared to control fibrinogen (Fig. 1b). The fibrinogen was fully oxidized by 150 μM HOCl with 70% reduction of polymerization rate. The maximal turbidity of the gels was also significantly decreased by HOCl oxidation, with the non-oxidized fibrin (0 μM HOCl) forming a very opaque gel and the HOCl-oxidized fibrin (150 μM HOCl) forming a transparent gel.

We then used thrombin time and reptilase time assays in a steel ball coagulometer to confirm that changes in turbidity represented a change in clot mechanics and structure rather than inhibition of clotting activation[22,23]. These assays are used to identify qualitative changes in fibrin polymerization (e.g., dysfibrinogenemia) and our previous studies had demonstrated sensitivity to the degree of oxidation[22,24]. Thrombin time measures the clotting time required for a clot to form at 37°C after addition of thrombin which activates the conversion of fibrinogen to fibrin by cleavage of fibrinopeptides A and B. Reptilase time uses batroxobin, a viper venom enzyme, as an alternative thrombin to confirm the presence of dysfibrinogenemia and measure the clotting time required for fibrinogen converted to fibrin by specific cleavage of fibrinopeptide A. Unlike thrombin, batroxibin is not sensitive to the effects of heparins. Like turbidity, both thrombin times and reptilase times were progressively prolonged by HOCl at 75 μM and higher concentrations compared to non-oxidized fibrinogen (Fig. 1c). Additionally, to add clinical relevance, the Clauss fibrinogen assay was performed to measure the concentration of functional fibrinogen. The modified Clauss fibrinogen assay is the most common clinical method used for clinical quantification of fibrinogen[23]. The concentrations of functional fibrinogen were significantly decreased with increasing HOCl oxidation in a dose-dependent manner (Fig. 1d). Again, fibrinogen solutions oxidized by 75 μM and higher HOCl concentrations induced functional fibrinogen levels below normally acceptable clinical ranges.

To confirm that oxidized fibrinogen could also disrupt clot formation in human plasma, we then tested the effects of adding HOCl-oxidized fibrinogen (pre-oxidation of purified fibrinogen by 150 μM HOCl) to normal pooled human plasma prior to clot formation. Again, the lag time was longer, the maximal slope of polymerization was decreased, and the rate of fibrin clot formation was decreased (Fig. 1e, f) in the presence of HOCl-oxidized fibrinogen. These results confirm that significant oxidation of fibrinogen in solution can disrupt fibrin formation in clinically relevant ways.

We then examined the effects of specifically blocking AαC domain interactions during fibrin polymerization for its similarity to HOCl oxidation by using a recombinant human AαC domain peptide fragment as a competitive inhibitor of AαC domain interactions. The fibrinogen alpha C domain[11] enhances lateral aggregation of protofibrils to form thick fibrin fibers[25,26]. MD simulations suggested that the oxidation of AαM476 knocks out fibrin protofibril lateral aggregation by shifting the equilibrium between open and closed conformation of the AαC domain in favor of the former[26]. We synthesized a homogeneous recombinant fibrinogen AαC419–502 (AαC fragment) corresponding to the human fibrinogen alpha C domain to be used as a specific competitive inhibitor of AαC domain interactions during fibrin polymerization. Protein BLAST analysis reported that the synthesized human AαC fragment shared 61% identity to the bovine sequence (Uniprot ID: P02672) and contained ordered structure at the N-terminal (Supplementary Fig. S1a). The AαC fragment was also confirmed to have one methionine residue at 476 and no tryptophan residues in its amino acid sequence (Supplementary Fig. S1a). Homology modeling of its 3D structure was also aligned with the human alpha C chain of fibrinogen (Uniprot ID: P02671) as analyzed by i-TASSER. The best predicted model of human AαC fragment is shown in the Supplementary Fig. S1b. The AαC fragment also showed a local concentration of negative charge at the N-terminal sub-domain and Met476 residue was exposed on the surface (Supplementary Fig. S1c). Since the alpha C domain is highly susceptible to proteolysis, we characterized the purity of the αC fragment by SDS-PAGE (Supplementary Fig. S2a) and confirmed its identity by ESI-TOF mass spectrometry analysis (Supplementary Fig. S2b).

We then clotted the purified fibrinogen using thrombin in the presence of increasing percentage of the AαC fragment. The final concentration of fibrinogen was maintained at 0.6 μM (2 mg/mL) at its lower physiological condition. Adding as little as 10% AαC fragment to native fibrinogen significantly decreased the maximum slope of fibrin polymerization, and maximal absorbance, which were considerably more affected in comparison to lag time (Fig. 1g, h). The impairment of clot structure was very similar to those measured in the presence of increasing HOCl oxidation (Fig. 1a vs. 1g), suggesting that HOCl oxidation and competitive inhibition of AαC domain interactions have similar disruptive effects on fibrin polymerization.

Oxidation alters fibrinogen structure and behavior in solution.

Fibrinogen monomers are made up of two sets of Aα, Bβ, and γ chains bound by disulfide bonds. As expected, we observed three bands corresponding to Aα (67 kDa), Bβ (55 kDa), and γ (45 kDa) chains on SDS-PAGE of the reduced control fibrinogen. Exposure of fibrinogen to increasing concentrations of HOCl up to 150 μM did not cause distinct changes in the electrophoretic banding pattern under reducing conditions (Supplementary Fig. S2c), suggesting that HOCl-induced oxidation does not fragment or significantly alter the molecular weight of individual fibrinogen chains.

CD spectroscopy was then utilized to investigate secondary structural changes of fibrinogen upon HOCl oxidation. The CD spectra of protein in the far ultraviolet (UV) range (180–250 nm) depends on the electronic excitation of the partially delocalized peptide bonds, which form the backbone of the polypeptide chain[27]. Therefore, changes in the main alpha helical peptide backbone structure of fibrinogen would be identifiable using this method. The far-UV CD spectra of the control and the oxidized fibrinogen (with an increasing HOCl concentration) showed similar characteristics of α-helical structure, exhibiting double negative bands at 222 and 208 nm (Supplementary Fig. S3a), suggesting that HOCl oxidation of fibrinogen did not alter its overall alpha helical backbone structure.

The hydrodynamic properties of fibrinogen in solution are concentration-dependent and largely determined by the intermolecular self-association of fibrinogen molecules mediated by the highly flexible and extensible αC regions[28]. The average hydrodynamic radii of control fibrinogen (0 μM HOCl) and the HOCl-oxidized fibrinogen solutions (150 μM HOCl) were 12.3 ± 0.08 nm and 12.2 ± 0.02 nm, respectively (Supplementary Fig. S3b). DLS analysis showed that fibrinogen oxidized by HOCl had similar correlation coefficient decay curves (Supplementary Fig. S3c). Regardless of HOCl oxidation, the purified fibrinogen solutions showed monodisperse scattering and the averaged hydrodynamic radii was not significantly different. These results suggest that the hydrodynamic size of fibrinogen as well as its secondary structure in prefibrillar state is only slightly affected by oxidation and are likely to be poorly predictive of fibrillar structural changes.

Fibrinogen diffusion in solution is largely determined by the intrinsic properties of the fibrinogen molecule which remain thermally stable in the 5–42°C temperature range under physiological conditions[28]. Since the fibrinogen solutions were homogenous and monodispersed regardless of HOCl oxidation, we measured ^{1}H spectra and translational diffusion of fibrinogen solutions in response to HOCl oxidation at 25°C by DOSY NMR analysis. Both control fibrinogen and oxidized fibrinogen solutions showed resonances with broad outline at amide and aliphatic regions in the ^{1}H spectra. The ^{1}H signals of fibrinogen solutions were dispersed at the amide region from 6.5 ppm to 8.5 ppm (Fig. S4a) and the fibrinogen methyl ^{1}H protons were observed at aliphatic region from 0.7 to 0.9 ppm (Fig. S4b). The signal amplitude of the fibrinogen methyl ^{1}H protons for the HOCl-oxidized fibrinogen solution (150 μM HOCl) was significantly lower than control fibrinogen (0 μM HOCl). The methyl signals in the upfield domain of the spectrum were then chosen for measurement of the diffusion coefficient of fibrinogen (Fig. S4b). DOSY NMR showed that the diffusion coefficients of control samples ^{1}H water and ^{1}H fibrinogen were $2.3 \pm 0.001 \times 10^{-11}$ m^2s^{-1} and $13.4 \pm 0.001 \times 10^{-11}$ m^2s^{-1}, respectively (Fig. S4c). This represents a ^{1}H water diffusion mobility two orders of magnitude slower than pure ^{1}H water proton which has been reported to be $2.3 \times 10^{-9} m^2 s^{-1}$ at 25°C[29], suggesting that water molecules became sequestered in the hydration shell of fibrinogen. Upon oxidation with 150 μM HOCl, the translational diffusion coefficient of ^{1}H water and ^{1}H fibrinogen were partially increased to $2.7 \times 10^{-11} \pm 0.001$ m^2s^{-1} and $14.5 \times 10^{-11} \pm 0.001$ m^2s^{-1}, respectively, demonstrating a 17.4% increased ^{1}H water diffusion mobility and 8.2% increased ^{1}H fibrinogen diffusion mobility (Fig. S4c). These results suggest that oxidized fibrinogen in solution has a more compact conformation and therefore enhanced translational mobility. However, the achievable stable detection limit of 50% oxidation likely lacks sensitivity and may not deliver a clinically usable diagnostic signature.

Oxidation alters T_2 relaxation of water protons in fibrinogen solution.

Two-dimensional D/T_2 and T_1/T_2 correlations were next used to determine correlations between NMR signatures (diffusion translational and T_2 relaxation) and architectural arrangement of fibrin clots. Water proton was used as a probe,

which allows monitoring of the two-dimensional D/T_2 correlations signals for simultaneous measurement of translational diffusion and T_2 relaxation using PFG and conventional CPMG with variable 2π delays. The 2D correlational spectrum in frequency domains was acquired and encoded sequentially over time. As compared to fibrinogen control solution (0 μM HOCl), the averaged translational diffusion coefficient of bulk water protons in the HOCl-oxidized fibrinogen solution (150 μM HOCl) was partially decreased from 4.64 $x10^{-9}$ m^2s^{-1} to 4.04 $x10^{-9}$ m^2s^{-1} (Supplementary Table S1, Fig. 2a) and the T_2 time was concomitantly decreased from 256.6 ms to 187.4 ms (Supplementary Table S1, Fig. 2b). Again, translational diffusion and T_2 time were minimally affected by oxidation of prefibrillar fibrinogen in solution.

To examine for similar effects of fibrinogen oxidation taking place in normal pooled human plasma, we determined the T_1/T_2 correlation profiles of water protons in plasma solutions before and after adding an increasing percentage of HOCl-oxidized fibrinogen (pre-oxidized by 150 μM HOCl). T_1 relaxation time did not contribute to surface relaxation of fibrinogen in the plasma (Supplementary Table S2, Fig. 2c). Increasing the fraction of oxidized fibrinogen significantly increased T_2 time of bulk water protons by 2-fold from 105 ms to 236 ms at a threshold of 50% HOCl-oxidized fibrinogen (Supplementary Table S2, Fig. 2d). There was a negative linear correlation between the T_2 relaxation rate of ^1H bulk water and the percentage of HOCl-oxidized fibrinogen added to the plasma (Fig. 2e), suggesting that oxidized fibrinogen molecules reoriented fibrinogen molecules to be less accessible by water molecules and thus prevented water-protein interaction.

Oxidation alters T_2 relaxation of water protons in fibrin clots.

We next used a 2D-NMR spectrometer to investigate the effects of HOCl oxidation on the structural rearrangements of fibrin clots. We first examined clots formed from HOCl-oxidized fibrinogen after their polymerization by thrombin. Compared to control fibrin gels, the translational diffusion coefficient of bulk water protons in the HOCl-oxidized fibrin gel (150 μM HOCl) partially decreased from 4.64 $x10^{-9}$ m^2s^{-1} to 3.51 $x10^{-9}$ m^2s^{-1} (Supplementary Table S1, Fig. 3a). In contrast, the T_2 relaxation time of bulk water protons increased from 211 ms to 377 ms (Supplementary Table S1, Fig. 3b) upon HOCl oxidation. The HOCl-oxidized fibrin gel demonstrated 2-fold increase of T_2 relaxation time and 24% reduction of translational diffusion, which may be attributed to thin and tightly packed fibrils in the oxidized fibrin gel relative to control[12]. These experiments also confirmed a threshold of detection for 2D-NMR of 12% oxidative change of fibrin structure arising from 25 μM HOCl exposure (Supplementary Table S1).

We next sought to determine the indirect effect of HOCl oxidation by addition HOCl-oxidized fibrinogen to human pooled plasma prior to clotting by measuring the T_1/T_2 correlation profiles of bulk water protons in the plasma fibrin gels containing an increasing percentage of pre-oxidized fibrinogen. T_1 relaxation was not affected by HOCl oxidation (Fig. 3c). However, bulk water protons in the 50% HOCl-oxidized plasma fibrin gel again shifted by 2-fold from 149 ms to 335 ms compared to controls (Supplementary Table S2, Fig. 3d) and was negatively correlated with the percentage of HOCl-oxidized fibrinogen added to plasma prior to clotting (Fig. 2e). Oxidation induced slow motion of water protons, favoring bulk water molecules attracted to hydration shells of the fibers in the plasma fibrin gel, leading to longer T_2 relaxation time that was consistent with direct oxidation of purified fibrinogen prior to clotting.

To further define water-protein interactions, including the hydration of fibers via water-water proton interaction, we next defined T_1/T_2 ratio as A-ratio to predict the degree of water-protein and/or water-water interactions as previously described[17]. Control plasma solutions demonstrated an A-ratio = 57.2 (Fig. 4a) that was distinctively larger than the highly oxidized plasma (50% HOCl-oxidized fibrinogen) (A-ratio = 21.5) (Fig. 4b). The T_2 distribution profiles showed that adding 50% HOCl-oxidized fibrinogen by volume to the plasma increased T_2 time by 2-fold from 123.3 ms to 46.4 ms (Supplementary Table S3, Fig. 4c). In addition, two distinct individual peaks were identified in the T_1/T_2 correlation spectrum, namely the S-peak which represented intermediate water molecules (T_{2i}) in the hydration shell of fibers, and R-

peak which represented bulk water (T_2) contained within the fibrin network of the gel (Fig. 4d). It is known that bulk water is an exchangeable peak[30] and a main contributor to surface relaxation[31]. The S-peak (T_2 = 81.1 ms, A-ratio = 37.7) in the 50% HOCl-oxidized plasma fibrin gel was substantially decreased and shifted to a longer T_2 time with a smaller A-ratio (Fig. 4e), attributing to the freely mobile bulk water molecules (R-peak) shifting towards the S-peak in the hydration layer of fibers via fast chemical exchange. This leads to an increase of hydration shell of the fibers in the oxidized plasma gel. The T_2 distribution profiles showed that adding 50% oxidized fibrinogen by volume to the plasma prior to clotting increased the intermediate water signal (T_{2i}) over 2-fold from 25.6 ms to 81.1 ms (Supplementary Table S3, Fig. 4f) and the T_2 relaxation rate of intermediate water (T_{2i}) was negatively correlated with the percentage of HOCl-oxidized fibrinogen added to plasma prior to clotting (Fig. 4g). This result supports increased water interactions within hydration shells with oxidation.

Lastly, we tested whether NMR relaxometry (low-field time domain benchtop NMR device operating at 80 MHz) could identify changes in the gel structure due to oxidation. Using this method, we detected an R-peak shift in the 50% HOCl-oxidized plasma gel to longer T_2 and an A-ratio that was relatively closer to the control plasma gel (Fig. 5a, b). This method also showed 2-fold longer T_2 time with higher signal intensity abundance than that of control (Fig. 5c). We found that NMR relaxometry could be used to distinguish oxidized fibrin gel from control, and its sensitivity was comparable to high filed NMR spectroscopy (Fig. 5d).

Discussion

Our results show that (i) NMR diffusion and relaxation of water can be used as a signature to detect alteration of fibrin clots due to the oxidation at the level of at least 12% or higher. (ii) We found that T_2 relaxation of water (and not T_1 or diffusion) can be used as the most sensitive readout correlated with oxidation. (iii) Detection can be achieved using high field NMR spectrometers as well as portable NMR systems operating at least 80 MHz. Measuring T_2 of water in the gel phase is typically fast and can be performed *in situ* within several minutes as opposed T_1 and diffusion requiring longer acquisition times. It was reported that total oxidation level in the plasma from patients with trauma coagulopathy was about 9% when focusing solely on methionine oxidation of soluble prefibrillar fibrinogen (*γ*M78, B*β*M367, and A*α*M476)[11,24]. Concentrations of neutrophils and fibrin at local wound sites may also have higher levels of oxidation, and fibrin becomes concentrated within clots, so that 2D NMR of fibrin clots may be sensitive to low level of oxidation when examining clotted fibrin samples, therefore overcoming limitations of using prefibrillar fibrinogen solutions.

Our results provide novel experimental evidence for the impact of oxidation on fibrinogen polymerization. These data support that HOCl oxidation alters fibrinogen polymerization similar to inhibition of AαC domain interactions during fibrin clot formation. Fibrinogen having truncated αC regions (Aα251) forms fibrin clots composed of thinner fibers, decreased stiffness, and enhanced fibrinolysis[12]. A recombinant hybrid fibrinogen variant in which the human αC regions were substituted with homologous chicken αC sequences lacked the ability to laterally aggregate beyond single-stranded protofibrils[13]. Competitive inhibition of lateral aggregation was also found in the presence of αC fragments[32]. We used a recombinant human αC fragment (AαC 419–502) as a titratable model of fibrin polymerization taking place without αC domain interactions. In each case, thin fibered clots having altered stiffness and susceptibility to fibrinolysis were the readout. Our results showed that the effect on clot turbidity was nearly identical to that seen with oxidation. This observation supports MD simulations pointing towards a potential mechanism by which oxidation of the AαC domain inhibits lateral protofibril aggregation due to partial burying of local polymerization binding sites[26] making lateral aggregation of fibrin monomers energetically unfavorable[33,34].

Water protons (^{1}H) are readily measured by 2D-NMR for detecting molecular and morphological changes of aggregates and complexes by proton T_1 and T_2 relaxation times[35]. T_2 relaxation time is governed mainly by proton-surface interactions and correlated to the morphological changes[18,36]. It can be utilized to identify different morphological

aggregate assemblies[37]. T_2 is sensitive to molecular dynamics of water and collagen structures in the extracellular matrix. For instance, an increase of T_2 was detected in articular cartilage degraded by collagen and loss of proteoglycan, resulting in an abnormal structural collage network[38]. Applying this approach to study fibrin clot structure after oxidation, we found that HOCl oxidation made fibrinogen less accessible to water molecules and prevented water-protein interactions, which may have direct effects of burying the active binding sites in the alpha C domains and inhibiting dimerization between fibrinogen molecules[33,34]. The total T_1/T_2 ratio of water protons was increased upon conversion of fibrinogen solution to plasma fibrin gel (refer to Fig. 4a, d), suggesting water-protein interactions for lateral aggregation of protofibrils and the amount of hydration was increased by gel formation. It has been reported that the hydration state changes during fibrin gel formation[39]. We have shown that T_2 relaxation in the fibrin gel was significantly affected by oxidation. T_2 relaxation rate of bulk water was inversely proportional to the density of fibers in the gel and thus it was increased by indirect oxidation. The motion of water molecules changed to be slower and restricted, attributing to high density of thin fibrils in the oxidized fibrin gel, which drastically increased T_2 relaxation time of bulk water protons. These changes are entirely consistent with direct structural analysis of HOCl oxidized fibrin gels demonstrating increased, tightly packed thin fibers and smaller pores[12]. Hence, T_2 relaxation is a promising surrogate of changes of fibril network structure[40] and fiber filament content.

We found that T_2 relaxation of bulk water reflected the structural changes of fibril arrangement and T_2 relaxation of intermediate water (T_{2i}) indicated the hydration of plasma fibrin gel. T_{2i} relaxation rate of intermediate water protons decreased with increasing of hydration shell of fibers in the plasma fibrin gels. The hydration of plasma fibrin gel was influenced by the extent of polymerization and cross-linking because of oxidation. Like the dipolar interactions induced by collagen fibril arrangements[38,40], hydration shell water molecules promote the stability of fibrin clot structure and provides additional water bridges between the fibers[40]. When the fibril network is impaired by oxidation, the rearrangement of fibrils can affect the relaxation characteristics of the fibrin gel. Thus, additional water hydration shells of HOCl oxidation altered morphological structure and likely contributed directly to mechanical softening of these gels as demonstrated previously[11].

We propose that T_2 relaxation of ^1H water can serve as a distinct NMR signature to detect the structural properties of the fibril network and provide morphological information on the structure. We anticipate that NMR relaxometry can be a potential device to rapidly identify the contribution of oxidation to coagulopathy after trauma.

Methods

Sample preparation

Human fibrinogen (plasminogen and von Willebrand depleted, 99% clottability) and human-α-thrombin were purchased from Enzyme Research Laboratories (#FIB 2). Human plasminogen (#16-16-161200, Athen Research and Technologies) and tranexamic acid (TXA) (Precision Technologies) were purchased. We purchase the commercially available recovered plasma frozen within 8 hours (#PS100, Seraplex Inc). Lyophilized human fibrinogen was dissolved in phosphate buffer saline (PBS; 137 M NaCl, 2.7 mM KCl, 8 mM $Na_2HPO_412H_2O$, 1.5 mM KH_2PO_4, and pH 7.4). Its concentration was determined spectrometrically at 278 nm using an extinction coefficient of 15.1 for 10 mg/mL solution[41]. Hypochlorous acid (HOCl) refers to a mixture of HOCl and OCl^- species. The hypochlorite concentration was determined spectrophotometrically using a wavelength of 292 nm ($\varepsilon = 350\ M^{-1}cm^{-1}$)[42]. All chemicals were of reagent grade and were purchased from Sigma-Aldrich, unless specified otherwise.

Fibrinogen Oxidation

The fibrinogen was incubated with different concentrations of HOCl (0, 10, 25, 50, 75, 100, 125, 150 µmol/L) for 1 h at 37°C. Fibrinogen was oxidized by HOCl at µmol/g of protein. The oxidation reaction was quenched with a 10 times molar excess of L-methionine. Non-oxidized fibrinogen (0 µmol HOCl) was used as control. The control sample was made to have the same composition as the 150 µmol/L oxidized sample by addition of methionine. After oxidation, the samples were separated into aliquots and stored at -80°C. The fibrin gel polymerization was prepared by adding $CaCl_2$ and thrombin to activate factor XIII and convert fibrinogen to fibrin. Unless otherwise stated, the final sample composition was 1 mg/mL fibrinogen, 0.16 NIH U/mL thrombin, 0.14 M NaCl, 44 mM HEPES, and 2 mM $CaCl_2$ in deionized water at pH 7.4, and gelation could proceed for at least 1 h before characterization was performed. It should be noted that the addition of methionine and HOCl, which were required for the oxidation reaction, caused a negligibly small increase (< 3%) in the ionic strength of the protein solutions. However, this small increase is not expected to significantly affect the fibrin gel morphology[43]. Fibrinogen concentration at 2 mg/mL in PBS, pH 7.4 was used in all the experiments, unless specified otherwise.

Circular Dichroism (CD)

Non-oxidized fibrinogen (0 µmol/L HOCl) and oxidized fibrinogen samples (10, 25, 50, 75, 100, 125, 150 µmol/L) were prepared at a concentration of 0.025 mg/mL in doubled distilled H_2O for CD spectra measurement (Chirascan™ V100). CD spectra of non-oxidized fibrinogen and oxidized fibrinogen samples were recorded at 25°C in 1 mm pathlength quartz cuvette from 270 to 195 nm. Triplicates were done with 0.5 µs time per incremental scan. Analysis of the CD spectra was performed using the secondary structure prediction program supplied with the spectropolarimeter. Molar ellipticity values [q] were calculated according to the equation: [θ] (deg-cm2 $dmol^{-1}$) = [θ (MRW)]/[10(l)(c)], where θ is the displacement from the baseline value X to the full range in degrees; MRW is the mean residue weight of the amino acids; (l) is the path length of the cell (cm); and (c) is protein concentration (g/mL). All CD data were expressed as the mean residue ellipticity [θ], in units of degrees square centimeter per decimole.

Spectrophotometric measurements

Fibrin polymerization was measured by monitoring turbidity changes with time at 350 nm at 37°C for 1h using UV-Vis spectrophotometer (Cytation™ 5 Cell Imaging Reader, Bio Tek). Fibrin polymerization was initiated by addition of 100 µL of 2x coating buffer (0.14 M NaCl, 2 mM $CaCl_2$, and 44 mM Hepes buffer) containing 0.16 NIH U/mL thrombin into 100 µL of oxidized or control fibrinogen. PBS was used as the blank. The process of fibrin formation can be described in terms of its individual components, including the rate of fibrinopeptide cleavage, protofibril formation, and finally the lateral assembly of protofibrils to form fibers. These processes can be measured kinetically using turbidimetric approaches, which are regularly used to determine fibrin clot assembly and structure[21]. Three portions of the turbidity curve are used to measure individual components contributing to fibrin polymerization. First, the initial lag phase represents the rate of fibrinopeptide cleavage by thrombin. The maximal slope of the polymerization curve (Vmax) indicates the rate of protofibril aggregation into fibers. Finally, the final absorbance reflects the fibrin fiber diameter, with increased turbidity correlating with thicker individual fibers[21].

SDS-PAGE

SDS-PAGE was performed according to Laemmli[44]. The electrophoretic pattern of fibrinogen upon HOCl oxidation was analyzed by SDS-PAGE. Reduced samples were prepared by adding 4x Laemmli sample buffer (Bio-Rad) containing 5% 2-mercaptoethanol and heated at 95ºC for 10 min. 5 µg of protein sample and 5 µL of protein marker (Precision Plus Protein™ Dual Color Standards) was loaded into the respective lane. Protein was separated on a 12% SDS-PAGE for 2 h at a constant voltage of 100V using Mini-PROTEAN® Tetra Cell (Bio-Rad). The gel was stained with Coomassie brilliant blue R-250 for 4 hours and destained in distilled water for 2 hours. Non-oxidized fibrinogen was used as a control.

Thrombin And Reptilase Time Assays

The STart Max coagulation analyzer (Diagnostica Stago) was used to measure the time required for a fibrin clot to form following the addition of a standard amount of thrombin and/or reptilase. Thrombin time measures the clotting time required for a clot to form at 37°C after the addition of thrombin which activates the conversion of fibrinogen to fibrin by cleavage of fibrinopeptides A and B. Reptilase time uses batroxobin, a viper venom, to measure the clotting time required for fibrinogen converted to fibrin by cleavage of fibrinopeptide A. The normal value of thrombin time and reptilase time are < 21 seconds and < 24 seconds, respectively.

Clauss Fibrinogen Assay (clottability)

The Clauss fibrinogen assay is used to measure the concentration of functional fibrinogen. It is performed on a dilution of fibrinogen samples to eliminate interference by substances such as heparin and fibrin degradation products. Sample was diluted at 1:20 with Owrens–Kohler. Fibrinogen concentration was quantified by addition of STA®-Liquid Fibrinogen reagent that containing human thrombin of 100 IU/mL to the diluted sample. The diluted fibrinogen is clotted with a high concentration thrombin, the resulting time to clot formation, typically measured either mechanically or optically, is directly proportional to the concentration of clottable fibrinogen in the sample. A standard curve of known fibrinogen concentration vs. clotting time is then used to determine the concentration of fibrinogen, of which fully functional fibrinogen is typically over 95% clottable. The STart Max coagulation analyzer (Diagnostica Stago) automatically converted the clotting time measured in seconds to fibrinogen concentration in mg/dL using a [log-log] fibrinogen standard curve. The normal fibrinogen level is at the range of 2–4 mg/mL (200–400 mg/dL).

Dynamic Light Scattering (DLS)

DLS analysis was performed at 25^{o}C using a Malvern Zetasizer Nano series instrument. DLS was used to determine the effect of HOCl oxidation on the hydrodynamic radius and size distribution of fibrinogen at physiological conditions i.e., 2 mg/mL at pH 7.4 and ionic strength of 0.15 M NaCl. The aggregation of fibrinogen with increasing concentration (2–10 mg/mL) were also determined.

Protein expression and purification of recombinant human AαC domain

A recombinant αC fragment corresponding to human fibrinogen αC-domain (Aα419–502 residues) was produced in *E. coli* using pET-28b expression vector as described earlier[45]. The pET-28b vector carrying the coding sequences of His-tagged Aα419–502 fragment was synthesized (Bio Basic Asia Pacific). It consisted of 6x His-linker-TEV cleavage (MGHHHHHHMGNSENLYFQ) and the coding sequences (GDKELRTGKEKVTSGSTTTTRRSCSKTVTKTVIGPDGHKEVTKEVVTSEDGSDCPEAMDLGTLSGIGTLDGFRHRHPDEAAFFDT). The plasmid was transformed into Rosetta™ 2(DE3) Singles™ *E. coli* host cells (Novagen). The cDNA fragment was sequenced in both directions to confirm the integrity of the coding sequences. Cells were grown in terrific broth at 37°C for 3–4 h until OD_{600} reached 0.8–1.0 and followed by induction with 0.5 mM Isopropyl β-D-1-thiogalactopyranoside (IPTG). The cells were induced and propagated at 18°C overnight. The cell pellet was harvested and dissolved in TBS (20 mM Tris-HCl buffer containing 150 mM NaCl and 0.1 mM PMSF, pH 8.0). The protein was then lysed by sonicator for several pulse cycles. The His-tagged Aα419–502 fragment was prepared from the soluble fraction of the bacterial lysate[45]. The soluble His-tagged protein was incubated with Ni-NTA resin at 4^{o}C overnight and purified through immobilized metal affinity chromatography (IMAC). The His-tagged Aα419–502 protein was eluted and concentrated using an Amicon ultra-15 centrifugal filter (molecular mass cutoff of 3 kDa) and desalted through a PD-10 column (GE Healthcare) equilibrated with TBS at pH 7.4. The recombinant protein was purified and fractionated by fast performance liquid chromatography (FPLC) (ÄKTA pure, GE Healthcare) on a Superdex75 10/300 GL column equilibrated with TBS at pH 7.4. The purified Aα419–502 protein was concentrated to 10–15 mg/mL using an Amicon ultra-15 centrifugal filter (Millipore) and stored at -80^{o}C prior analysis. Purity of native Aα419–502 fragment (without reduction by 2-mercaptoethanol) was analyzed by 15% SDS-PAGE.

Protein Concentration Determination

Concentration of the recombinant human Aα419–502 fragment was determined spectrophotometrically at 280 nm using extinction coefficient $E^{1\%}$ = 1.27 calculated from the amino acid composition with the equation: $E^{1\%}$ = (5,690W + 1,280Y + 120S-S)/(0.1M), where W, Y and S-S represent the number of Trp and Tyr residues and disulfide bonds, respectively, and M represents the molecular mass[46]. The amino acids sequence of the recombinant human AαC419–502 fragment was analyzed by ProParam (Swiss-Prot software).

Mass Spectrometry Analysis

The intact Aαc 419–502 fragment was prepared, and its molecular mass was determined by ESI-TOF mass spectrometer for molecular mass determination of proteins (Agilent Technologies). The samples were analyzed by the Proteomic Core Facility of the Biological Research Center (BRC). The data was acquired at the rate of 1 spectrum/sec and the acquisition window was set from *m/z* 100 to 3000. The peaks in the total ion chromatogram (TIC) were integrated and the mass spectra at 180 fragmentor voltages were obtained. The multiple charge state distributions of the intact proteins were deconvoluted using the Maximum Entropy deconvolution algorithm.

NMR measurement of translational diffusion

The ^{1}H DOSY (diffusion-ordered spectroscopy) experiments were carried out at 25^{o}C on a Bruker DRX 600-MHz spectrometer equipped with a cryoprobe and a standard *z*-gradient inverse probe head (TXI, 5 mm tube) capable of producing gradients with a maximum strength of 53 G/cm. ^{1}H DOSY composed of a stimulated-echo sequence incorporating bipolar gradient pulses and a longitudinal eddy current delay (PFG)[47] was used for self-diffusion measurement. The water signal was suppressed by the means of pre-saturation. The amplitude of field gradient was varied from 2–95% of G_{max} over 32 steps increment under constant diffusion time (50 ms). A gradient recovery delay of 0.2 ms and an eddy current delay of 5 ms were used. Sample for DOSY experiment was prepared by addition of 10% D_2O (v/v) and 0.5 mM 4, 4- dimethyl-4-silapentane-1-sulfonic acid (DSS) to the unlabeled fibrinogen with or without HOCl oxidation. The chemical shift region 0.9 – 0.6 ppm that encompassed strong signals for fibrinogen methyl protons was chosen for measurements of the translational diffusion. This region was selected to eliminate potential errors in the peak integrals arising from disturbances of the water signal and to avoid extra complications from overlapping signals. The chemical shifts of the ^{1}H resonances were referenced to DSS signal. Data processing using the Bruker Topspin 3.5 software and the translational diffusion was analyzed by NMRgenerator[48] and computer-aided resonance assignment (CARA)[49].

NMR measurement of ^{1}H proton diffusion/T_2 and T_1/T_2 relaxation times

Plasma spiked with non-oxidized and oxidized fibrinogen were supplemented with 10% D_2O. Samples were gently mixed and transferred into 3 mm NMR tubes. Fibrin gels were prepared by addition of 1.0 µL of 0.2 mol/L $CaCl_2$ solution and 1.0 µL of thrombin (final concentration 0.4 NIH U/mL) to 200 µL of plasma spiked with non-oxidized and oxidized fibrinogen. Samples were gently mixed and transferred into 3 mm NMR tube and equilibrated at 37°C for 5 min. The samples were used for NMR measurements of diffusion/transverse (D/T_2) and longitudinal/transverse (T_1/T_2) relaxation correlations of water protons. NMR measurements were performed on a Bruker Avance III 600 MHz spectrometer. Diffusion data were acquired using PFG with encoding delay of 1 ms, diffusion delay of 50 ms, and maximum gradient strength of 53 G/cm. T_1/T_2 correlation data were acquired using a Carr-Purcell-Meiboom-Gill (CPMG)[19] and saturation inversion recovery pulse sequences with echo time of $2{\cdot}\tau_2$ = 1.92 ms, and inversion time τ_1 logarithmically spaced from 1 ms to 50 s. The number of echo for T_1 and T_2 were 32 and 38, respectively. The accumulated signals were collected from 1 scan of the data points in the multi-dimensional spectra. Firstly, the multi-dimensional NMR data were acquired using a conventional CPMG with

variable 2τ delays and saturation recovery pulse trains. Next, we also acquired multi-dimensional T_1/T_2 correlations using modified CPMG with shorter 2τ delays and saturation inversion recovery pulse sequences. Echo signals were acquired between two adjacent 180^o pulses. The fast acquisition of T_1 /T_2 correlations were obtained and analyzed by 2D inverse Laplace transform. Whereas the saturation inversion recovery and conventional CPMG decay curves were analyzed by 2D inverse Laplace transform algorithm (2DILT) and Iterative Thresholding Algorithm for Multiexponential Decay (ITAMeD) to deconvolute multiple D/T_2 or T_1/T_2 signals as previously described[50,51]. These algorithms exploit the principle of compressed sensing for sparse sampling, processing, resolving, and reconstruction of the D/T_2 and T_1/T_2 correlations. The accumulated signal intensity data were converted to logarithms. CONTIN-generated translational diffusion, T_1 and T_2 profiles were obtained from the continuous ILT of the multi-exponential decay curves. The number of exponential decays was fixed to three for all samples. Water T_2 was the dominant component, accounting for > 90% of the total CPMG signal intensity[19]. T_1 and T_2 correlations were analyzed by the software under MATLAB.

NMR relaxometry

The water proton T_1/T_2 relaxation times of native plasma fibrin gel and plasma fibrin gel spiked with 50% oxidized fibrinogen were measured using a Bruker mq20 Minispec benchtop relaxometry operating at 0.47 T, corresponding to 20 MHz for measurement of T_1/T_2 relaxations of ^{1}H water proton. Plasma fibrin gels containing 10% D_2O were prepared in a 5 mm NMR tube and firmly fixed into a 10 mm NMR tube. The sample height was 1 cm, corresponding to a total volume of 50 µL. The temperature of samples was equilibrated to 25°C and NMR relaxometry measurement was performed at 298 K. A modified saturation inversion recovery and CPMG[19] pulse sequences were used for measurement of longitudinal/transverse (T_1/T_2) relaxation correlations. Eight scans were used for the signal averaging in each experiment, and 36 data points collection time of 1 min echo time and 6000 number of echoes.

Electrostatic Potential Calculations

The electrostatic potential maps of AαC 419–502 were calculated at experimental conditions (150 mM NaCl ionic strength at pH 7.4, 25^{o}C) using the adaptive Poisson–Boltzmann solver (APBS) plugin in PyMOL. The input PQR files were generated by PDB2PQR server. The grid dimensions were automatically set by the APBS plugin according to the dimensions of input AαC 419–502 structure. The electrostatic potentials were calculated by solving the nonlinear Poisson-Boltzmann equation with a single Debye and Hückel (DH) sphere boundary condition. The solvent accessible surface area was calculated using a solvent radius of 1.4 Å. The secondary structure model of AαC 419–502 was predicted by i-TASSER.

Statistical analysis

All experiments were performed in triplicate from three independent experiments unless otherwise stated. Data were expressed as mean ± standard deviation. The comparison between HOCl oxidation of fibrinogen and controls were assessed using the ANOVA-Bonferroni test. The statistically significant difference vs control was at the $P < 0.05$ level. The correlation between the T_2 relaxation rate and plasma fibrinogen solution/ fibrin gel with addition of HOCl-oxidized fibrinogen was analyzed by Pearson correlation. All the data were analyzed using Excel and GraphPad Prism (GraphPad Software).

Declarations

Acknowledgements

We would like to thank Dr. Mateusz Urbańczyk (University of Oulu, Finland) for providing 2D Inverse Laplace Transformation and compressed sensing MATLAB script. We acknowledged Bruker BioSpin GmbH for providing the NMR relaxometry and Dr. Marcio-Fernando Cobo (Bruker BioSpin GmbH, Rheinstetten, Germany) for invaluable discussions and

technical assistance in the sample measurement and analysis. We also acknowledged Proteomic Core Facility of the Biological Research Center (BRC, NTU) for ESI-TOF MS analysis of the recombinant human αC construct. This work was funded by NTU Integrated Medical Biological and Environmental Life Sciences (NIMBELS), project reference: NIM/05/2016 (30/06/2017 to 29/12/2019).

Author contributions

W.H.L designed the experimental plan, performed the experiments, analyzed the data, and wrote the manuscript. N.J.W provided insightful suggestions and guidance on the project. K.P devised the NMR studies and supervised the project. T.W.Y and R.L.G supported the work with materials and facilities. T.W.Y and R.L.G also provided advice on the project. W.H.L, N.J.W, and K.P. reviewed and revised the manuscript. All authors reviewed, revised, and approved the manuscript.

Competing interests

The authors declare no competing interests.

Data availability statement

The datasets generated and/or analyzed during the current study are available from the corresponding author on reasonable request.

References

1 Weisel, J. W. & Litvinov, R. I. Fibrin Formation, Structure and Properties. *Subcell Biochem* **82**, 405-456, doi:10.1007/978-3-319-49674-0_13 (2017).

2 Kollman, J. M., Pandi, L., Sawaya, M. R., Riley, M. & Doolittle, R. F. Crystal structure of human fibrinogen. *Biochemistry* **48**, 3877-3886, doi:10.1021/bi802205g (2009).

3 Brown, J. H., Volkmann, N., Jun, G., Henschen-Edman, A. H. & Cohen, C. The crystal structure of modified bovine fibrinogen. *Proceedings of the National Academy of Sciences* **97**, 85, doi:10.1073/pnas.97.1.85 (2000).

4 Weisel, J. W. & Litvinov, R. I. Mechanisms of fibrin polymerization and clinical implications. *Blood* (2013).

5 Weisel, J. W. & Medved, L. The structure and function of the alpha C domains of fibrinogen. *Annals of the New York Academy of Sciences* **936**, 312-327 (2001).

6 Weisel, J. W. Fibrinogen and fibrin. *In Advances in protein chemistry* **70**, 247-299, doi:10.1016/S0065-3233(04)70008-X (2005).

7 Gorkun, O. V., Veklich, Y. I., Medved, L. V., Henschen, A. H. & Weisel, J. W. Role of the alpha C domains of fibrin in clot formation. *Biochemistry* **33**, 6986-6997 (1994).

8 Prokopowicz, Z. M. *et al.* Hypochlorous acid: a natural adjuvant that facilitates antigen processing, cross-priming, and the induction of adaptive immunity. *Journal of immunology (Baltimore, Md. : 1950)* **184**, 824-835, doi:10.4049/jimmunol.0902606 (2010).

9 Rosen, H. *et al.* Methionine oxidation contributes to bacterial killing by the myeloperoxidase system of neutrophils. *Proceedings of the National Academy of Sciences of the United States of America* **106**, 18686-18691, doi:10.1073/pnas.0909464106 (2009).

10 Locke, M., Francis, R. J., Tsaousi, E. & Longstaff, C. Fibrinogen protects neutrophils from the cytotoxic effects of histones and delays neutrophil extracellular trap formation induced by ionomycin. *Sci Rep* **10**, 11694-11694, doi:10.1038/s41598-020-68584-0 (2020).

11 Weigandt, Katie M. *et al.* Fibrin Clot Structure and Mechanics Associated with Specific Oxidation of Methionine Residues in Fibrinogen. *Biophysical Journal* **103**, 2399-2407, doi:https://doi.org/10.1016/j.bpj.2012.10.036 (2012).

12 Gorkun, O. V., Henschen-Edman, A. H., Ping, L. F. & Lord, S. T. Analysis of A alpha 251 fibrinogen: the alpha C domain has a role in polymerization, albeit more subtle than anticipated from the analogous proteolytic fragment X. *Biochemistry* **37**, 15434-15441, doi:10.1021/bi981551t (1998).

13 Ping, L. *et al.* Substitution of the human alphaC region with the analogous chicken domain generates a fibrinogen with severely impaired lateral aggregation: fibrin monomers assemble into protofibrils but protofibrils do not assemble into fibers. *Biochemistry* **50**, 9066-9075, doi:10.1021/bi201094v (2011).

14 Strumwasser, A. *et al.* The impact of acute coagulopathy on mortality in pediatric trauma patients. *Journal of Trauma and Acute Care Surgery* **81** (2016).

15 Davies, E. *et al.* Dynamics of water in agar gels studied using low and high resolution 1H NMR spectroscopy. *International Journal of Food Science & Technology* **45**, 2502-2507, doi:https://doi.org/10.1111/j.1365-2621.2010.02448.x (2010).

16 Filippi, M. & Agosta, F. Magnetic resonance techniques to quantify tissue damage, tissue repair, and functional cortical reorganization in multiple sclerosis. *Progress in brain research* **175**, 465-482, doi:10.1016/s0079-6123(09)17531-3 (2009).

17 Peng, W. K., Ng, T.-T. & Loh, T. P. Machine learning assistive rapid, label-free molecular phenotyping of blood with two-dimensional NMR correlational spectroscopy. *Communications Biology* **3**, 535, doi:10.1038/s42003-020-01262-z (2020).

18 Skewis, L. R. *et al.* T2 Magnetic Resonance: A Diagnostic Platform for Studying Integrated Hemostasis in Whole Blood - Proof of Concept. *Clinical Chemistry* **60**, 1174-1182, doi:10.1373/clinchem.2014.223735 (2014).

19 Cistola, D. P. & Robinson, M. D. Compact NMR relaxometry of human blood and blood components. *Trends Analyt Chem* **83**, 53-64, doi:10.1016/j.trac.2016.04.020 (2016).

20 Cines, D. B. *et al.* Clot contraction: compression of erythrocytes into tightly packed polyhedra and redistribution of platelets and fibrin. *Blood* **123**, 1596-1603, doi:10.1182/blood-2013-08-523860 (2014).

21 Weisel, J. W. & Nagaswami, C. Computer modeling of fibrin polymerization kinetics correlated with electron microscope and turbidity observations: clot structure and assembly are kinetically controlled. *Biophysical journal* **63**, 111-128, doi:10.1016/S0006-3495(92)81594-1 (1992).

22 Martinez, M., Weisel, J. W. & Ischiropoulos, H. Functional impact of oxidative posttranslational modifications on fibrinogen and fibrin clots. *Free radical biology & medicine* **65**, 411-418, doi:10.1016/j.freeradbiomed.2013.06.039 (2013).

23 Mackie, I. J. *et al.* Guidelines on fibrinogen assays. *British Journal of Haematology* **121**, 396-404, doi:https://doi.org/10.1046/j.1365-2141.2003.04256.x (2003).

24 White, N. J. *et al.* Post-translational oxidative modification of fibrinogen is associated with coagulopathy after traumatic injury. *Free radical biology & medicine* **96**, 181-189, doi:10.1016/j.freeradbiomed.2016.04.023 (2016).

25 Tsurupa, G. *et al.* On the Mechanism of αC Polymer Formation in Fibrin. *Biochemistry* **51**, 2526-2538, doi:10.1021/bi2017848 (2012).

26 Burney, P. R., White, N. & Pfaendtner, J. Structural Effects of Methionine Oxidation on Isolated Subdomains of Human Fibrin D and αC Regions. *PLOS ONE* **9**, e86981, doi:10.1371/journal.pone.0086981 (2014).

27 Greenfield, N. J. Using circular dichroism spectra to estimate protein secondary structure. *Nature protocols* **1**, 2876-2890, doi:10.1038/nprot.2006.202 (2006).

28 Zuev, Y. F. *et al.* Conformational Flexibility and Self-Association of Fibrinogen in Concentrated Solutions. *The Journal of Physical Chemistry B* **121**, 7833-7843, doi:10.1021/acs.jpcb.7b05654 (2017).

29 Holz, M., Heil, S. R. & Sacco, A. Temperature-dependent self-diffusion coefficients of water and six selected molecular liquids for calibration in accurate 1H NMR PFG measurements. *Physical Chemistry Chemical Physics* **2**, 4740-4742, doi:10.1039/B005319H (2000).

30 Dortch, R., Horch, R. & Does, M. Development, simulation, and validation of NMR relaxation-based exchange measurements. *The Journal of chemical physics* **131**, 164502 (2009).

31 McDonald, P., Korb, J.-P., Mitchell, J. & Monteilhet, L. Surface relaxation and chemical exchange in hydrating cement pastes: a two-dimensional NMR relaxation study. *Physical Review E* **72**, 011409 (2005).

32 Veklich, Y. I., Gorkun, O. V., Medved, L. V., Nieuwenhuizen, W. & Weisel, J. W. Carboxyl-terminal portions of the alpha chains of fibrinogen and fibrin. Localization by electron microscopy and the effects of isolated alpha C fragments on polymerization. *The Journal of biological chemistry* **268**, 13577-13585 (1993).

33 Pederson, E. N. & Interlandi, G. Oxidation-induced destabilization of the fibrinogen α; C-domain dimer investigated by molecular dynamics simulations *Proteins: Structure, Function, and Bioinformatics.*, doi:10.1101/452912 (2019).

34 Pederson, E. N. & Interlandi, G. Effects of inflammation-induced oxidation on the dimerization of fibrinogen αC domain. *bioRxiv* (2018).

35 Wiesman, Z. *et al.* 2D and 3D Spectrum Graphics of the Chemical-Morphological Domains of Complex Biomass by Low Field Proton NMR Energy Relaxation Signal Analysis. *Energy & Fuels* **32**, 5090-5102, doi:10.1021/acs.energyfuels.7b03339 (2018).

36 Luo, Z.-X., Fox, L., Cummings, M., Lowery, T. J. & Daviso, E. New frontiers in in vitro medical diagnostics by low field T2 magnetic resonance relaxometry. *TrAC Trends in Analytical Chemistry* **83**, 94-102, doi:https://doi.org/10.1016/j.trac.2016.02.025 (2016).

37 Song, Y. Q. *et al.* T1–T2 Correlation Spectra Obtained Using a Fast Two-Dimensional Laplace Inversion. *Journal of Magnetic Resonance* **154**, 261-268, doi:https://doi.org/10.1006/jmre.2001.2474 (2002).

38 Nieminen, M. T. *et al.* Quantitative MR microscopy of enzymatically degraded articular cartilage. *Magnetic resonance in medicine* **43**, 676-681, doi:https://doi.org/10.1002/(SICI)1522-2594(200005)43:5<676::AID-MRM9>3.0.CO;2-X (2000).

39 Tanaka, Y. *et al.* Hydration of fibrinogen, fibrin, and fibrin degradation product (FDP) as estimated by nuclear magnetic resonance (NMR) spectroscopy. *Blood coagulation & fibrinolysis : an international journal in haemostasis and thrombosis* **2**, 243-249, doi:10.1097/00001721-199104000-00005 (1991).

40 Gründer, W., Wagner, M. & Werner, A. MR-microscopic visualization of anisotropic internal cartilage structures using the magic angle technique. *Magnetic resonance in medicine* **39**, 376-382, doi:https://doi.org/10.1002/mrm.1910390307 (1998).

41 Carr, M. E. & Hermans, J. Size and Density of Fibrin Fibers from Turbidity. *Macromolecules* **11**, 46-50, doi:10.1021/ma60061a009 (1978).

42 Morris, J. C. The Acid Ionization Constant of HOCl from 5 to 35°. *The Journal of Physical Chemistry* **70**, 3798-3805, doi:10.1021/j100884a007 (1966).

43 Yeromonahos, C., Polack, B. & Caton, F. Nanostructure of the Fibrin Clot. *Biophysical Journal* **99**, 2018-2027, doi:https://doi.org/10.1016/j.bpj.2010.04.059 (2010).

44 Laemmli, U. K. Cleavage of structural proteins during the assembly of the head of bacteriophage T4. *Nature* **227**, 680 (1970).

45 Matsuka, Y. V., Medved, L. V., Migliorini, M. M. & Ingham, K. C. Factor XIIIa-Catalyzed Cross-Linking of Recombinant αC Fragments of Human Fibrinogen. *Biochemistry* **35**, 5810-5816, doi:10.1021/bi952294k (1996).

46 Gill, S. C. & von Hippel, P. H. Calculation of protein extinction coefficients from amino acid sequence data. *Analytical biochemistry* **182**, 319-326, doi:10.1016/0003-2697(89)90602-7 (1989).

47 Wu, D. H., Chen, A. D. & Johnson, C. S. An Improved Diffusion-Ordered Spectroscopy Experiment Incorporating Bipolar-Gradient Pulses. *Journal of Magnetic Resonance, Series A* **115**, 260-264, doi:https://doi.org/10.1006/jmra.1995.1176 (1995).

48 Irvine, A. G., Slynko, V., Nikolaev, Y., Senthamarai, R. R. P. & Pervushin, K. Collaborative development for setup, execution, sharing and analytics of complex NMR experiments. *Journal of Magnetic Resonance* **239**, 121-129, doi:https://doi.org/10.1016/j.jmr.2013.12.004 (2014).

49 Keller, R. *The Computer Aided Resonance Assignment*. (2004).

50 Urbańczyk, M., Bernin, D., Koźmiński, W. & Kazimierczuk, K. Iterative Thresholding Algorithm for Multiexponential Decay Applied to PGSE NMR Data. *Analytical Chemistry* **85**, 1828-1833, doi:10.1021/ac3032004 (2013).

51 Urbanczyk, M., Kozminski, W. & Kazimierczuk, K. Accelerating diffusion-ordered NMR spectroscopy by joint sparse sampling of diffusion and time dimensions. *Angewandte Chemie (International ed. in English)* **53**, 6464-6467, doi:10.1002/anie.201402049 (2014).

Figures

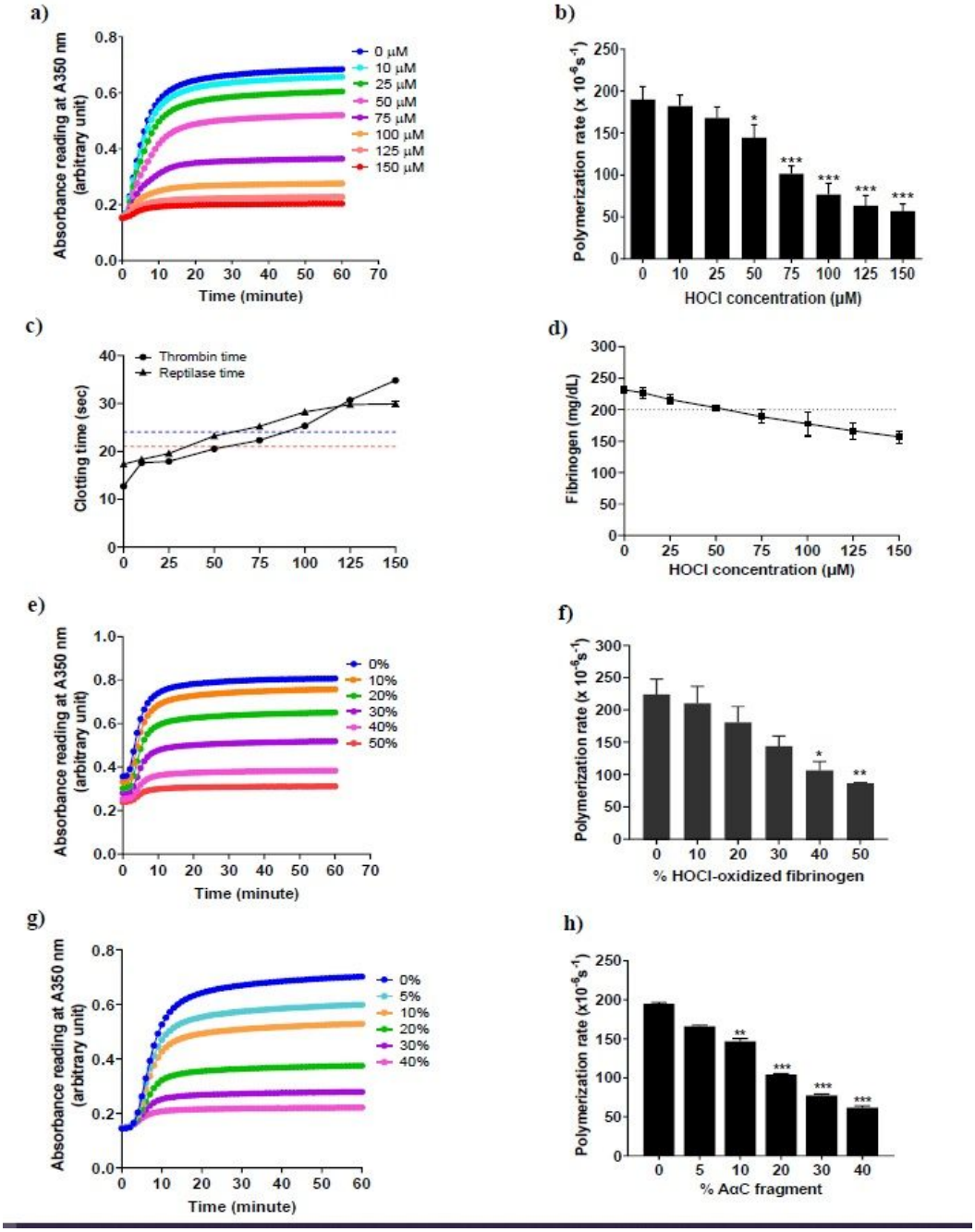

Figure 1

(a) Turbidity curves of non-oxidized fibrinogen (0 µM HOCl) and purified fibrinogen solutions oxidized with an increasing HOCl concentrations (10, 25, 50, 75, 100, 125, 150 µM). Non-oxidized fibrinogen (0 µM HOCl) was used as control. Fibrin polymerization was measured by monitoring turbidity changes with time at 350 nm wavelength at 37°C for 1 hour using UV-Vis spectrophotometer. The absorbance reading of the turbidity was recorded every 10 minutes interval for 60 minutes. Lag time represents the time required to form protofibrils, and maximum rate of polymerization represents the rate of protofibril assembly into fibers. (b) Maximum rate of polymerization for control fibrinogen and the fibrinogen solutions oxidized with increasing HOCl concentrations (10, 25, 50, 75, 100, 125, 150 µM). (c) Thrombin and reptilase times for the control fibrinogen and fibrinogen solutions oxidized with increasing HOCl concentrations. Thrombin and reptilase time measured the clotting time needed for fibrin clot formation after addition of thrombin and reptilase, receptively. The normal value of thrombin time and reptilase time are < 21 seconds and < 24 seconds, respectively. The red and blue dotted lines indicate the upper limit of the thrombin and reptilase times that required for normal fibrin clot formation. (d) Clauss

fibrinogen was used to measure the concentration of functional fibrinogen in the control fibrinogen and purified fibrinogen solutions oxidized with an increasing HOCl. The normal fibrinogen level is at the range of 2 - 4 mg/mL (200 - 400 mg/dL). The black dotted line indicates the upper limit of normal fibrinogen concentration. (e) Turbidity curves of control plasma fibrinogen and plasma fibrinogen solution added with an increasing level of HOCl-oxidized fibrinogen (10, 20, 30, 40, and 50%). Plasma fibrinogen solution without oxidized fibrinogen (0% oxidized fibrinogen in the plasma) was used as control. (f) Maximum rate of polymerization for control plasma fibrinogen and plasma fibrinogen solution added with an increasing HOCl-oxidized fibrinogen (pre-oxidation of purified fibrinogen by 150 μM HOCl). (g) Turbidity curves of control fibrinogen and the purified fibrinogen solutions added with an increasing percentage of AαC fragment (5, 10, 20, 30, and 40%). The copolymerization of the protein mixtures was activated by incubation with 0.16 NIH U/mL thrombin at 37oC for 1 hour. (h) Maximum rate of polymerization of control fibrinogen and the purified fibrinogen added with an increasing percentage of AαC fragment. P values that were 0.05 and less were considered statistically significant, as assessed using ANOVA-Bonferroni test. * P<0.05; ** P<0.01; *** P<0.001.

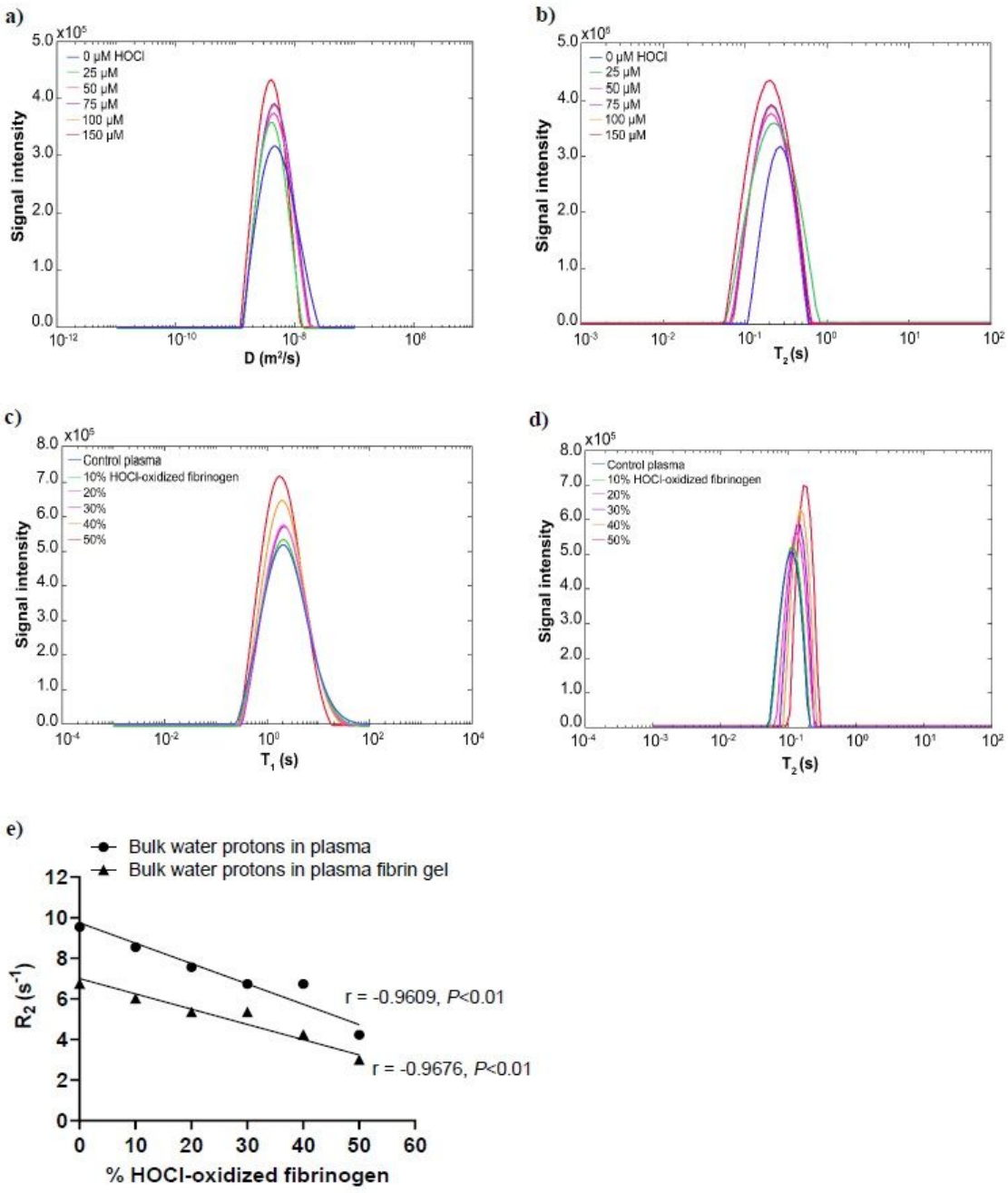

Figure 2

Diffusion/T2 correlations of 1H water in the purified fibrinogen solutions oxidized by increasing HOCl concentrations (25, 50, 75, 100, 150 μM). The D/T2 correlations were simultaneously measured by PFG for translational diffusion coefficient (D) and conventional CPMG for T2 relaxation time. (a) Translational diffusion (D) distributions of bulk water in the control fibrinogen and the purified fibrinogen solutions oxidized by increasing HOCl concentrations. (b) T2 distributions of bulk water in the control fibrinogen and the purified fibrinogen solutions oxidized by increasing HOCl concentrations. Non-oxidized fibrinogen solution (0 μM HOCl) was used as a control fibrinogen. (c) T1 distributions of bulk water in the control plasma and plasma added with an increasing percentage of HOCl-oxidized fibrinogen (10, 20, 30, 40, 50%) (pre-oxidation of purified fibrinogen by 150 μM HOCl). (d) T2 distributions of bulk water in the control plasma and plasma added with an increasing percentage of HOCl-oxidized fibrinogen. Plasma without HOCl-oxidized fibrinogen (0%) was used as control plasma. Plasma was indirectly oxidized by adding HOCl-oxidized fibrinogen (10, 20, 30, 40, 50%). The T1/T2 correlations were simultaneously measured by saturation inversion recovery for T1 time and conventional CPMG for T2 relaxation time. (e) T2 relaxation (R2) of bulk 1H water in response to indirect oxidation by adding HOCl-oxidized fibrinogen to the plasma solutions and the plasma fibrin gels prior to clotting. The correlation of T2 relaxation with the percentage of HOCl-oxidized fibrinogen added to plasma as well as the plasma fibrin gels prior to clotting. The correlations of T2 relaxation were analyzed by Pearson correlations. P< 0.05 is considered as a significant correlation. The 2D-NMR diffusion/T2 correlations and T1/T2 were measured using 600 MHz NMR spectrometer. The multiple D/T2 or T1/T2 water signals analyzed by 2D inverse Laplace transform algorithm (2DILT) and Iterative Thresholding Algorithm for Multiexponential Decay (ITAMeD).

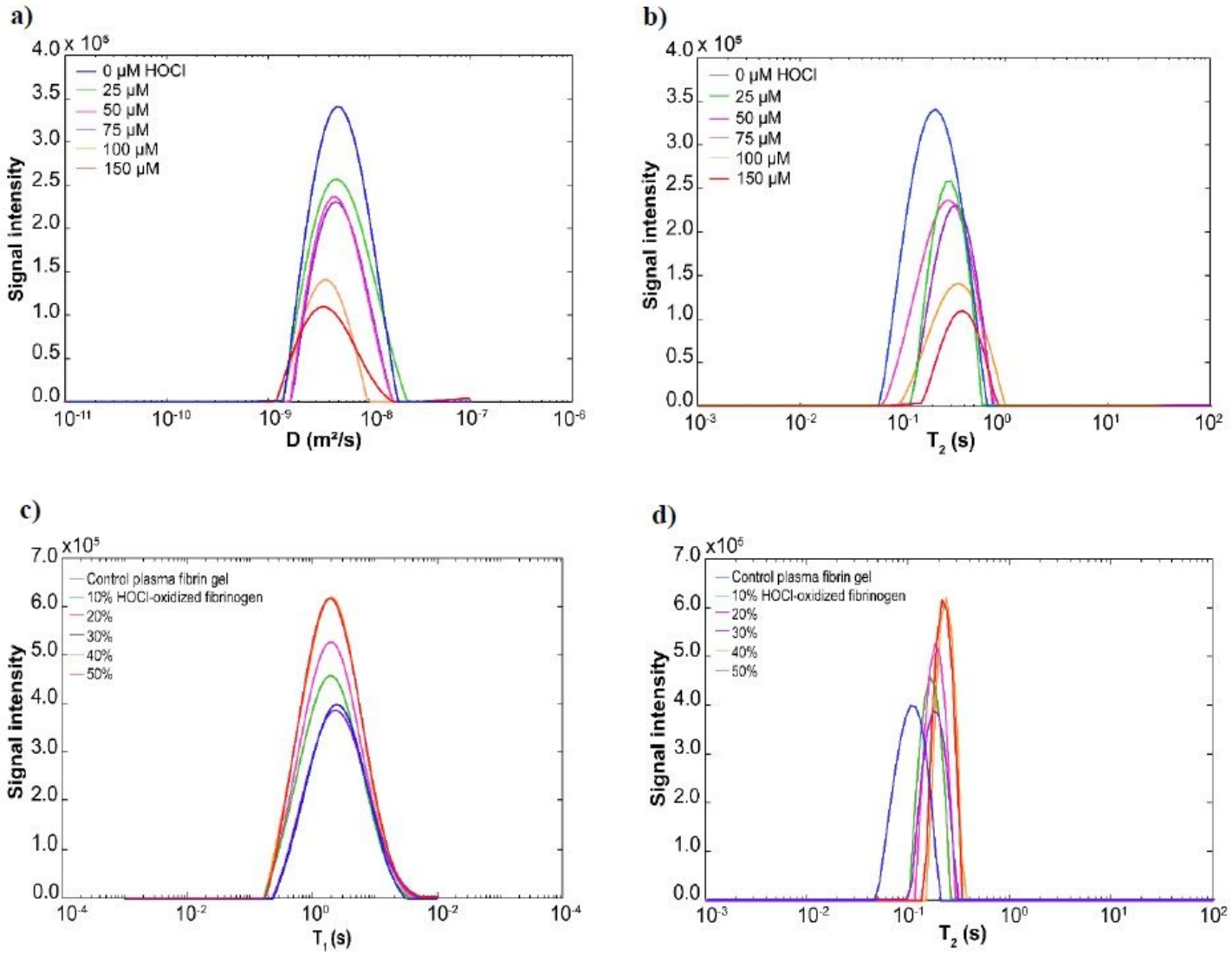

Figure 3

Diffusion/T2 correlations of 1H water protons in the fibrin gels oxidized by increasing HOCl concentrations (25, 50, 75, 100, 150 μM). The D/T2 correlations were simultaneously measured by PFG for translational diffusion coefficient (D) and conventional CPMG for T2 relaxation time. (a) Translational diffusion (D) distributions of bulk water in the fibrin gel and fibrin gels directly oxidized by increasing HOCl concentrations. (b) T2 distributions of bulk water in the fibrin gel and fibrin gels directly oxidized by increasing HOCl concentrations. Non-oxidized fibrin gel (0 μM HOCl) was used as control. (c) T1 distributions of bulk water in the control plasma and plasma added with an increasing percentage of HOCl-oxidized fibrinogen (10, 20, 30, 40, 50%). (d) T2 distributions of bulk water in the control plasma gel and plasma fibrin gels added with an increasing percentage of HOCl-oxidized fibrinogen. Plasma gel without HOCl-oxidized fibrinogen (0%) was used as control. Plasma was indirectly oxidized by adding HOCl-oxidized fibrinogen (10, 20, 30, 40, 50%) to plasma prior clotting. The HOCl-oxidized plasma fibrin gels were formed by adding HOCl-oxidized fibrinogen and then incubated with 0.16 NIH U/mL thrombin at 37oC for 1 hour. The T1/T2 correlations were simultaneously measured by saturation inversion recovery for T1 time and conventional CPMG for T2 relaxation time.

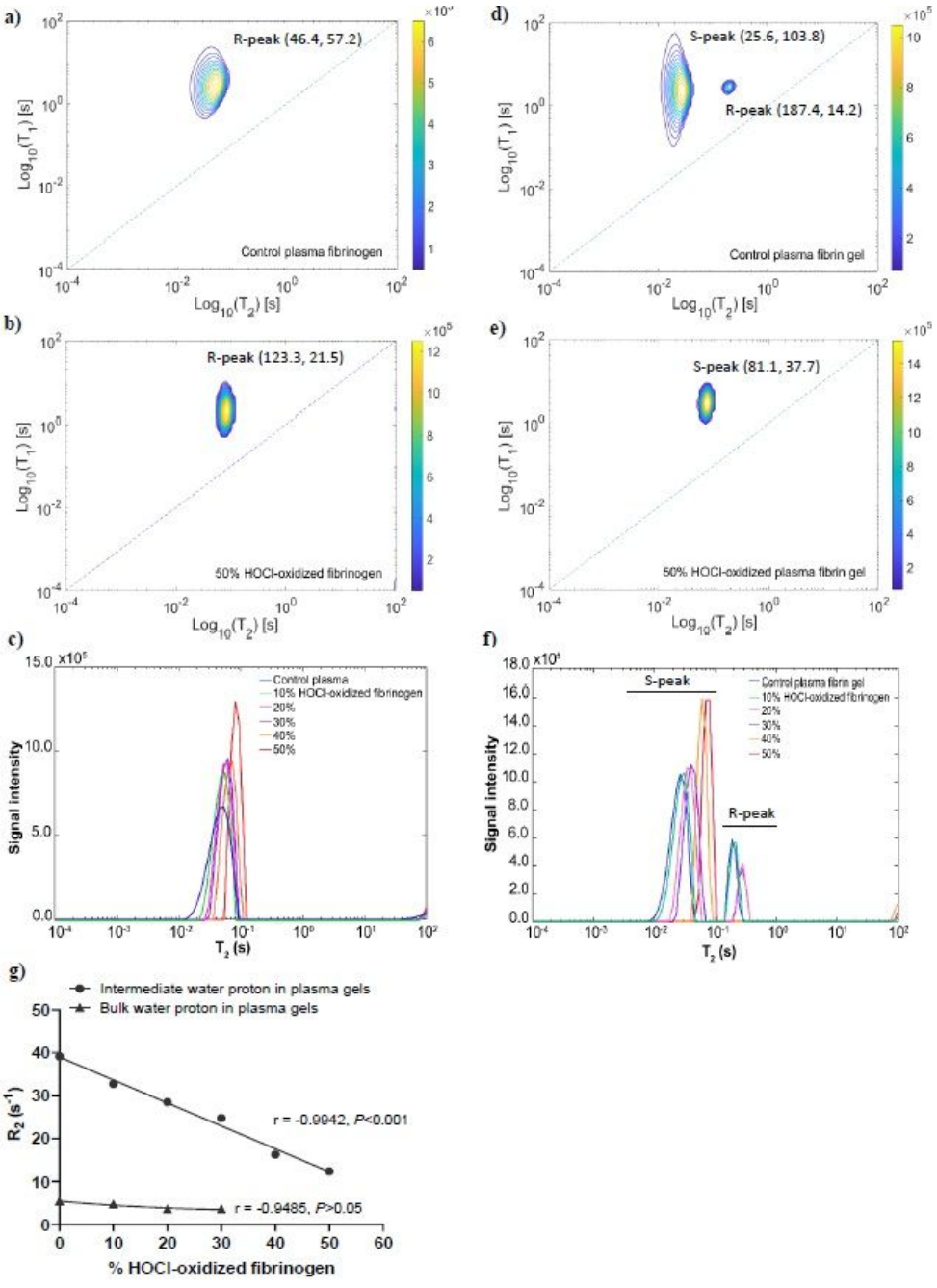

Figure 4

The 2D T2/T2 correlational spectra of control plasma and 50% HOCl-oxidized plasma solutions (added with 50% HOCl-oxidized fibrinogen) were measured by fast acquisition with a modified CPMG. (a) 2D T2/T2 correlational spectrum of control plasma. (b) 2D T2/T2 correlational spectrum of 50% HOCl-oxidized plasma solution. The R-peak was bulk water molecules within the fibrin network of the gel. The coordinate is represented as (T2 relaxation (in ms), A-ratio (unitless)). A-ratio was the ratio of T1/T2. (c) T2 distributions of bulk water in the plasma solution and plasma solutions added with an increasing percentage of HOCl-oxidized fibrinogen (10, 20, 30, 40, 50%) (pre-oxidation of purified fibrinogen by 150 μM HOCl). (d) 2D T2/T2 correlational spectrum of control plasma fibrin gel. (e) 2D T2/T2 correlational spectrum of 50% HOCl-oxidized plasma fibrin gel (added with 50% HOCl-oxidized fibrinogen prior to clotting). The decomposed multiple relaxation components in the T1/T2 correlational spectrum, including the bulk water that resided in the gel (R-peak), intermediate water was present in the hydration shell of fibers (S-peak). T1/T2 correlational spectrum was in the semilog-log plot. The unbound pure water molecule is located on the diagonal line (A-ratio approaches unity). (f) T2 distributions of 1H water in the control plasma gel and plasma fibrin gels added with increasing of HOCl-oxidized fibrinogen solutions (10, 20, 30, 40, 50%) prior to clotting. The 1H intermediate water (T2i) and 1H bulk water (T2) were found in the control plasma fibrin gels. Plasma fibrin gel without HOCl-oxidized fibrinogen (0%) was used as control. The fast acquisition of T1 /T2 correlations were analyzed by 2D inverse Laplace transform. (g) The correlations between T2 relaxation of 1H water and the indirect oxidation of plasma fibrin gels by adding HOCl-oxidized to plasma prior to clotting. T2 relaxation (R2) of intermediate and bulk water protons in response to an increasing percentage of HOCl-oxidized fibrinogen added to plasma prior to clotting. The correlations of T2 relaxation of 1H water was analyzed by Pearson correlations. $P < 0.05$ is considered as a significant correlation.

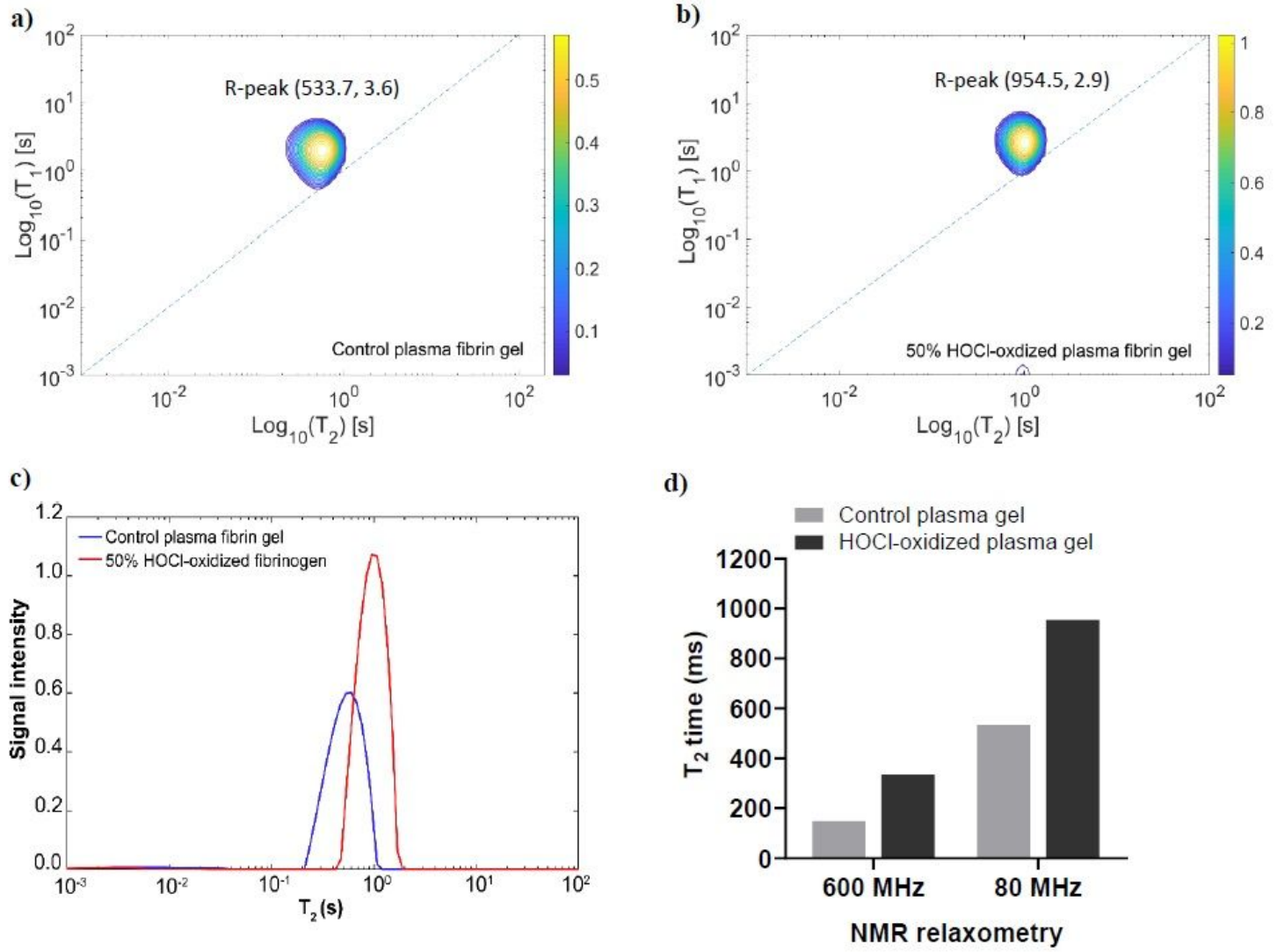

Figure 5

The 2D T2/T2 correlational spectra of control plasma fibrin gel and 50% HOCl-oxidized plasma fibrin gel were measured by 80 MHz NMR relaxometry. (a) 2D T2/T2 correlational spectrum of control plasma fibrin gel. (b) 2D T2/T2 correlational spectrum of 50% HOCL-oxidized plasma fibrin gel (added with 50% oxidized fibrinogen prior to clotting). The R-peak was bulk water molecules within the fibrin network of the gel. The coordinate is represented as (T2 relaxation (in ms), A-ratio (unitless)). A-ratio is the ratio of T1/T2. (c) T2 distributions of 1H water signal in the control plasma gels and 50% HOCl-oxidized plasma fibrin gels. (d) T2 relaxation times of the control plasma gel and 50% HOCl-oxidized plasma fibrin gel measured by 80 MHz and 600 MHz NMR relaxometry. The 80 MHz relaxometry acquired eight scans for the signal averaging in each experiment, 36 data points collection time of 1 min echo time, and 6000 number of echoes. The 600 MHz spectrometer used a modified CPMG and saturation inversion recovery pulse sequences with echo time of 2·τ2 = 1.92 ms, and inversion time τ1 logarithmically spaced from 1 ms to 50 s. The number of echo for T1 and T2 were 32 and 38, respectively.

Supplementary Files

This is a list of supplementary files associated with this preprint. Click to download.

- SupplementaryInformationRevised.pdf